

# Quintom-like transit universe models in Metric-affine Myrzakulov $f(R, T, Q, T_m)$ gravity

Dinesh Chandra Maurya<sup>1</sup>, Harjit Kumar<sup>2</sup>

<sup>1</sup>Centre for Cosmology, Astrophysics and Space Science, GLA University, Mathura-281 406, Uttar Pradesh, India.

<sup>2</sup>P.G. Department of Mathematics, S U College, Hilsa(Nalanda), Bihar, Patliputra University, Patna, Bihar.

<sup>1</sup>E-mail:dcmaurya563@gmail.com

<sup>2</sup>E-mail:harjeetkumar01@gmail.com

## Abstract

The current transit universe model is a precise solution to the equations of a new type of gravity theory called metric-affine Myrzakulov  $f(R, T, Q, T_m)$  [Herko et al. *Phys. Dark Univ.* **34** (2021) 100886]. We find a hyperbolic solution and determine the limits on the model's parameters using the latest observational data. We examine how certain cosmological factors, like the deceleration parameter  $q(z)$ , effective equation of state parameter  $\omega_{eff}$ , dark energy equation of state parameter  $\omega_{de}$ , and matter energy density parameter  $\Omega$ , change over time to help explain the properties of the observable universe. We establish a hyperbolic solution and obtain the observational constraints on the model parameters using the latest observational datasets. We study the evolution of several cosmological parameters, including the deceleration parameter  $q(z)$ , effective equation of state (EoS) parameter  $\omega_{eff}$ , dark energy EoS parameter  $\omega_{de}$ , to explain the properties of the observable universe. We perform the Om diagnostic test for the model, and it represents the phantom scenarios of the model. The behavior of the dark energy EoS parameter  $\omega_{de}$  reveals the quintom-A-type universe characteristics.

**Keywords:** Metric-affine Myrzakulov  $f(R, T, Q, T_m)$  gravity; Quintom-like universe; Transit universe; Exact cosmology; Observational constraints.

PACS number: 98.80-k, 98.80.Jk, 04.50.Kd

## Introduction

The rapid expansion of the cosmos during both early and late epochs [1–7] poses challenges for explanation within the framework of general relativity (GR). This disparity between theory and observations has led to the development of various theories beyond GR, collectively known as “Modified Gravity” [8]. The exploration of a viable alternative has proven advantageous and informative for our comprehension of gravity. Modified gravity theories encompass metric formulations. Various gravitational theories include  $f(R)$  theories, Metric-Affine (Palatini)  $f(R)$  gravity [9–11], teleparallel  $f(T)$  gravities [12, 13], symmetric teleparallel  $f(Q)$  [14–17], and scalar-tensor theories [18, 19] among others. The selection of alterations is mostly based on personal preference. We believe that the most attractive options are those that add to the basic geometry of spacetime by providing a wider connection than the traditional Levi-Civita connection. In the absence of a priori restrictions on the connection, the space is typically not Riemannian [20] and will exhibit both torsion and non-metricity. It is considered an additional fundamental field that overlays the metric. Determining the affine relationship facilitates the computation of the final geometric quantities. Metric-affine gravity theories have been formulated on this non-Riemannian manifold [21]. Recently, [22] examined  $f(R)$  gravity theories utilizing symmetric, torsion-free connections. These are known as Palatini  $f(R)$  theories of gravity. U4 theories represent gravitational frameworks characterized by torsion and the

absence of non-metricity. Reference [23] examines the dynamics of metric-affine gravity theories, whereas reference [24] analyzes the dynamics of generalized Palatini gravity theories. The metric-affine variational concepts in GR are examined in [25]. Recently, the role of non-metricity in metric-affine gravity theories was investigated [26].

The Metric-Affine technique has become increasingly prominent in recent years, particularly in relation to its applications in cosmology [27–38]. This attention may be due to a basic geometrical understanding of the other implications that operate in this context, unlike GR. The observed alterations are entirely due to non-metricity and spacetime torsion. Furthermore, geometric interpretations are encouraged by matter with intrinsic structure [29] and [39–42]. The connection between generalized geometry and inner structure offers a further benefit to the MAG approach. The affinely connected metric theories, especially the Riemann-Cartan subclass [43], justify the development of cosmological models utilizing a particular, albeit non-unique, connection. The simultaneous inclusion of non-zero curvature and torsion enhances the degrees of freedom necessary for gravitational alterations [44]. The evolution of the early and late universes can be explained by metric-affine gravity [45–49]. This paradigm was used in a recent cosmology study [45] to examine the temporal changes of observable quantities including density parameters and the effective dark energy equation-of-state parameter. Using the mini-super-space technique, the study analyzed cosmic behavior, highlighting the influence of the connection, and introducing the theory as a distortion of GR and its teleparallel counterpart. Reference [50] examined the observational constraints associated with Metric-Affine  $F(R, T)$ -gravity. Metric-affine gravity theories and their applications are detailed in [51–57].

Motivated by the foregoing talks, we create some FLRW cosmological models in a generalized metric-affine matter-geometry coupling theory that was recently proposed by Harko et al. [58]. We studied transit phase cosmological models in Metric-Affine  $F(R, T)$  gravity with observational constraints [59]. In [60, 61], we investigated certain exact cosmological models in the metric-affine  $F(R, T)$  gravity while a dark energy model in metric-affine  $f(R, Q)$  gravity is discussed in [62]. In this study, we are considering at different FLRW cosmological models and their attributes using the Metric-Affine  $f(R, T, Q, T_m)$  gravity theory.

The present paper is organized as follows: Section 1 is introductory, and section 2 contains a brief review of Metric-affine Myrzakulov  $f(R, T, Q, T_m)$  gravity theory. The field equations are given in section 3, while some cosmological exact solutions are presented in section 4. The observational analyses are given in section 5, and result discussions are shown in section 6. Finally, the conclusions are given in section 7.

## 2 Metric-affine $f(R, T, Q, T_m)$ gravity

We analyze the following action for the metric-affine gravity theory  $f(R, T, Q, T_m)$  [58].

$$S = \int \sqrt{-g} d^4x [f(R, T, Q, T_m) + L_m], \quad (1)$$

where  $f$  represents a function dependent on the Ricci curvature scalar  $R$ , the torsion scalar  $T$ , the nonmetricity scalar  $Q$ , and the trace  $T_m$  of the energy-momentum tensor (EMT) of the matter  $T_{ij}$  derived from the matter Lagrangian  $L_m$ . The gravitational theory formulated from the action (1) seeks to unify the various theories represented by  $f(R)$  [63],  $f(T)$  [64],  $f(Q)$  [65],  $f(R, T_m)$  [66],  $f(T, T_m)$  [67], and  $f(Q, T_m)$  [68, 69].

The current theory of gravity is formulated within a metric-affine manifold  $(M, g_{ij}, \Gamma_{ij}^\rho)$ . Consequently, we present the associated general metric-affine connection  $\Gamma_{ij}^\rho$  as [58]

$$\Gamma_{ij}^\rho = \check{\Gamma}_{ij}^\rho + K_{ij}^\rho + L_{ij}^\rho. \quad (2)$$

In the context of Riemann geometry, the Levi-Civita connection  $\check{\Gamma}_{ij}^\rho$  is associated, while the contorsion tensor  $K_{ij}^\rho$  relates to torsional geometry, and the disformation tensor  $L_{ij}^\rho$  pertains to nonmetricity geometry.

The definition of these tensors is as follows:

$$\check{\Gamma}^\alpha_{\beta\gamma} = \frac{1}{2}g^{\alpha\rho}(\partial_\gamma g_{\beta\rho} + \partial_\beta g_{\gamma\rho} - \partial_\rho g_{\beta\gamma}), \quad (3)$$

$$K_{ij\alpha} = \frac{1}{2}(T_{ij\alpha} + T_{j\alpha i} - T_{\alpha ij}), \quad (4)$$

$$S_\alpha^{ij} = \frac{1}{2}(K^{ij}{}_\alpha + \delta^i_\alpha T^{\beta j}{}_\beta - \delta^j_\alpha T^{\beta i}{}_\beta), \quad (5)$$

$$L_{\alpha ij} = \frac{1}{2}(Q_{\alpha ij} - Q_{ij\alpha} - Q_{ji\alpha}). \quad (6)$$

The non-metricity and twisting tensors have been added as

$$T^\alpha_{ij} = 2\Gamma^\alpha_{[ij]}, \quad Q_{\rho ij} = \nabla_\rho g_{ij}. \quad (7)$$

In a metric-affine spacetime, the introduction of the three scalars occurs as follows

$$R = g^{ij}R_{ij}, \quad (8)$$

$$T = S_\rho^{ij}T^\rho_{ij}, \quad (9)$$

$$Q = L^\alpha_{\beta\alpha}L^{\beta i}{}_i - L^\alpha_{\beta i}L^{\beta i}{}_\alpha. \quad (10)$$

In this context,  $R$  represents the curvature scalar associated with the Weyl-Cartan geometry, while  $T$  denotes the torsion scalar, and  $Q$  indicates the nonmetricity scalar. The Ricci tensor is derived from the affine connection based on its conventional definition.

$$R_{j\beta} = \partial_i \Gamma^i_{j\beta} - \partial_j \Gamma^i_{i\beta} + \Gamma^i_{i\alpha} \Gamma^\alpha_{j\beta} - \Gamma^i_{j\alpha} \Gamma^\alpha_{i\beta}. \quad (11)$$

By varying the action Eq. (1) with respect to both the connection and the metric, we derive the subsequent two field equations. [70]

$$\begin{aligned} & f_R \left[ g_{i[j} Q_{\alpha]\beta}{}^\beta + T_{i\alpha j} + Q_{\alpha ij} - g_{\alpha i} Q_{\beta j}{}^\beta \right] + f_Q \left[ 2g_{i(j} L^\beta_{\alpha)\beta} + g_{\alpha j} (L_{i\beta}{}^\beta - L^\beta_{i\beta}) - 2L_{i\alpha j} \right] \\ & + f_T \left[ T_{\alpha ij} + T_{i\alpha j} - T_{j\alpha i} + g_{\alpha[j} T^{\beta}{}_{i]\beta} \right] + 2g_{i[\alpha} \nabla_{j]} f_R - \frac{1}{2} H_{\alpha ij} = 0, \end{aligned} \quad (12)$$

and

$$\begin{aligned} & f_R R_{ij} - \frac{1}{2} f g_{ij} + f_{T_m} (g_{ij} L_m - T_{ij}) - \frac{1}{2} T_{ij} - \frac{1}{2} \nabla_\alpha \left( A^\alpha_{(ij)} - A_{(i}{}^\alpha{}_{j)} + A_{(ij)}{}^\alpha \right) \\ & + \frac{1}{4} f_T \left[ 2T_{\alpha j\beta} T^\alpha{}_i{}^\beta + 2T^\alpha{}_i{}^\beta T_{\beta j}{}^\alpha - 4T^\alpha_{i\alpha} T^\beta_{j\beta} - T_i{}^\alpha{}^\beta T_{j\alpha\beta} \right] \\ & + \frac{1}{4} f_Q \left[ 3Q_\alpha{}^\beta{}_\beta Q^\alpha_{ij} - g_{ij} Q_{\alpha\beta}{}^\beta Q^{\alpha\gamma}{}_\gamma - 2Q_{\alpha j\beta} Q^\alpha{}_i{}^\beta + 2Q^\alpha{}_i{}^\beta Q_{\beta j\alpha} - 2Q^\alpha_{i\alpha} Q^\beta_{j\beta} \right. \\ & \left. + Q_{\beta(i}{}^\beta Q_{j)\alpha}{}^\alpha - 2Q_\alpha{}^\beta{}_\beta Q_{(ij)}{}^\alpha + Q_i{}^\alpha{}^\beta Q_{j\alpha\beta} \right] = 0, \end{aligned} \quad (13)$$

correspondingly, where the energy-momentum tensor and the hypermomentum tensor are defined by

$$T_{ij} = -\frac{2}{\sqrt{-g}} \frac{\delta(\sqrt{-g} L_m)}{\delta g^{ij}}, \quad H_\lambda{}^{ij} = -\frac{2}{\sqrt{-g}} \frac{\delta(\sqrt{-g} L_m)}{\delta \Gamma^\lambda_{ij}}. \quad (14)$$

Furthermore, we have established

$$A_{i\alpha j} = f_Q (g_{ij} L^\beta_{\alpha\beta} + g_{\alpha j} L_{i\beta}{}^\beta - L_{i\alpha j} - L_{j\alpha i}). \quad (15)$$

All curvature terms and derivatives are derived from the affine connection  $\Gamma^\alpha_{ij}$ .

We will now present the Weyl vector, beginning with a straightforward formulation of the non-metricity tensor, which we will define as follows.

$$Q_{ij\alpha} = w_i g_{j\alpha}. \quad (16)$$

In this context,  $w_i$  represents the Weyl vector. The gravitational field equations of the  $f(R, T, Q, T_m)$  theory, in this instance, reduce to

$$\begin{aligned} & f_T [T_{\alpha ij} - g_{\alpha[i} T_{j]\beta}^{\beta} + T_{i\alpha j} - T_{j\alpha i}] \\ & + f_Q [2g_{\alpha(j} w_{i)} - 2g_{i(\alpha} w_{j)}] \\ & + f_R [T_{i\alpha j} - 2g_{i[\alpha} w_{j]}] + 2g_{i[j} \nabla_{\alpha]} f_R - \frac{1}{2} H_{\alpha ij} = 0, \end{aligned} \quad (17)$$

and

$$\begin{aligned} & f_R R_{ij} - \frac{1}{2} f g_{ij} + f_{T_m} (g_{ij} L_m - T_{ij}) - \frac{1}{2} T_{ij} - g_{ij} w^\alpha \nabla_\alpha f_Q + w_{(j} \nabla_{i)} f_Q \\ & + \frac{1}{2} f_Q [\nabla_{(i} w_{j)} - 5g_{ij} w^\alpha w_\alpha - w_i w_j - g_{ij} \nabla_\alpha w^\alpha - g_{\alpha(i} \nabla_{j)} w^\alpha] \\ & + \frac{1}{4} f_T [2T_{\alpha j \beta} T_{i \alpha}^{\alpha \beta} + 2T_{i \alpha}^{\alpha \beta} T_{\beta j}^{\beta \alpha} - 4T_{i \alpha}^{\alpha} T_{j \beta}^{\beta} - T_{i \alpha}^{\alpha \beta} T_{j \beta \alpha}] = 0, \end{aligned} \quad (18)$$

in that order. At this juncture, it is important to observe that in the equations presented above, all curvature terms and their derivatives are derived from the affine connection  $\Gamma_{ij}^\alpha$ .

The torsion tensor  $T_{ij\alpha}$  can be expressed in a decomposed form as

$$T_{ij\rho} = \frac{2}{3}(t_{ij\rho} - t_{\rho j i}) + (A_j g_{i\rho} - A_\rho g_{ij}) + \epsilon_{ij\rho\sigma} B^\sigma, \quad (19)$$

where  $t_{ij\alpha}$  represents a tensor characterized by the following properties,

$$t_{ij\rho} + t_{j\rho i} + t_{\rho i j} = 0, \quad t^i{}_{ij} = 0 = t^i{}_{ji}, \quad (20)$$

and  $3A_i = T_{i\alpha}^\alpha$ , where  $B_i$  represents two arbitrary vectors. This study will operate under the assumption that solely the  $A_i$  vector is non-zero. The torsion tensor can therefore be expressed as

$$T_{ij\alpha} = A_j g_{i\alpha} - A_\alpha g_{ij}. \quad (21)$$

The equations governing the field exhibit simplification in this scenario as

$$\begin{aligned} & 8f_T g_{\alpha[i} A_{j]} + 2f_Q [g_{\alpha(j} w_{i)} - g_{i(j} w_{\alpha)}] \\ & + 2f_R [g_{i[j} A_{\alpha]} - g_{i[\alpha} w_{j]}] + 2g_{i[\alpha} \nabla_{j]} f_R = 0, \end{aligned} \quad (22)$$

and

$$\begin{aligned} & f_R \check{R}_{ij} - \frac{1}{2} f g_{ij} + f_{T_m} (g_{ij} L_m - T_{ij}) - \frac{1}{2} T_{ij} - g_{ij} w^\alpha \check{\nabla}_\alpha f_Q + w_{(j} \check{\nabla}_{i)} f_Q - f_T A_i A_j \\ & + \frac{1}{2} f_Q [3A^\alpha w_\alpha g_{ij} - 2g_{ij} w_\alpha w^\alpha - 3A_{(i} w_{j)} + 2w_i w_j - 2g_{ij} \check{\nabla}_\alpha w^\alpha + 2\check{\nabla}_{(i} w_{j)}] \\ & + \frac{1}{2} f_R [2(A_\alpha A^\alpha g_{ij} - A_i A_j) + A^\alpha w_\alpha g_{ij} + 2A_{(i} w_{j)} + w_i w_j - w^\alpha w_\alpha g_{ij} \\ & - g_{ij} \check{\nabla}_\alpha (2A^\alpha - w^\alpha) + \check{\nabla}_{(i} A_{j)} + \check{\nabla}_{(i} w_{j)}] = 0, \end{aligned} \quad (23)$$

in that order. The equations provided include all curvature terms and derivatives obtained from the Levi-Civita connection  $\check{\Gamma}_{ij}^\alpha$ . On the other hand, we have proposed that the energy-momentum tensor of the matter field is derived exclusively from the metric tensor and is not influenced by the affine connection.

For future reference, we can note that the torsion, non-metricity, and curvature scalars can be expressed as

$$\begin{aligned} T &= -6A^2, \quad Q = -\frac{3}{2}w^2, \\ R &= \check{R} + 3A^2 + 3A_\alpha w^\alpha - \frac{3}{2}w^2 - 3\check{\nabla}_i A^i + 3\check{\nabla}_i w^i, \end{aligned} \quad (24)$$

with  $A^2 \equiv A_\alpha A^\alpha$  and  $w^2 \equiv w_\alpha w^\alpha$ .

### 3 Field equations

The Friedmann-Lemaitre-Robertson-Walker (FLRW) metric is examined in its conformal coordinates representation, which is expressed as follows

$$ds^2 = a^2(t) (-dt^2 + d\vec{x}^2), \quad (25)$$

where  $a = a(t)$  represents the conformal scale factor. The Hubble parameter is introduced, defined as  $H = \dot{a}/a$ . It is posited that the matter sector of the Universe can be characterized by a perfect fluid, with the equations of motion derivable from the Lagrangian  $L_m = -\rho$ , and which possesses the energy-momentum tensor.

$$T^\mu_\nu = \text{diag}(-\rho, p, p, p). \quad (26)$$

In this context,  $\rho$  represents the energy density, while  $p$  denotes the thermodynamic pressure.

Given the homogeneity and isotropy of space-time, the expressions for the Weyl and torsion vectors can be formulated as

$$\begin{aligned} A_\mu &= (aA_0, \vec{0}), \\ w_\mu &= (aw_0, \vec{0}), \end{aligned} \quad (27)$$

where  $A_0 = A_0(t)$  and  $w_0 = w_0(t)$  represent two functions that vary with time. The equation of motion pertaining to the affine connection is presented here. Equation (22) consists of two independent components, which correspond to the Weyl vector and the torsion vector. These can be simplified as follows:

$$\begin{aligned} f_R(A_0 + w_0) - f_Q w_0 &= \frac{1}{a} \dot{f}_R, \\ 4f_T A_0 - f_Q w_0 &= 0. \end{aligned} \quad (28)$$

The generalized Friedman and Raychaudhuri equations can be derived as follows [70]

$$a^2 \left[ f + 2A_0^2 f_T - 3A_0 w_0 f_R \right] + a \left[ \dot{w}_0 + H w_0 \right] f_Q + a \left[ \dot{A}_0 - \dot{w}_0 + H(A_0 - w_0) \right] f_R - 6(\dot{H} + H^2) f_R = a^2 \rho \quad (29)$$

and

$$\begin{aligned} a^2 f - 2(\dot{H} + 3H^2) f_R + 2a^2(\rho + p) f_{T_m} + 2aw_0 \dot{f}_Q + a \left[ 2\dot{w}_0 + w_0(2H + 2aw_0 - 3aA_0) \right] f_Q \\ - a \left[ \dot{w}_0 - 2\dot{A}_0 + a(2A_0 - w_0)(A_0 + w_0) - (2A_0 - w_0)H \right] f_R = -a^2 p, \end{aligned} \quad (30)$$

respectively.

## 4 Cosmological solutions

In this study, we consider the linear form of arbitrary function  $f(R, T, Q, T_m)$  as [58]

$$f(R, T, Q, T_m) = \frac{1}{2}R + \alpha T + \beta Q + \gamma T_m, \quad (31)$$

where  $\alpha$ ,  $\beta$  and  $\gamma$  are coupling arbitrary constants. From Eq. (31), we get the partial derivatives as

$$f_R = \frac{1}{2}, \quad f_T = \alpha, \quad f_Q = \beta, \quad f_{T_m} = \gamma. \quad (32)$$

Using Eq. (32) in (28), we obtain the following relations

$$\begin{aligned} A_0 - (2\beta - 1)w_0 &= 0, \\ 4\alpha A_0 - \beta w_0 &= 0. \end{aligned} \quad (33)$$

Solving Eq. (33), we obtain the solution either

$$A_0 = 0, w_0 = 0, \quad (34)$$

or

$$A_0 = (2\beta - 1)k, \quad w_0 = k, \quad (35)$$

with condition  $\alpha = \frac{\beta}{2\beta-1}$ .

In the first case, the solution (34) reveals that both torsion and nonmetricity vanishes together, and hence, we get  $f(R, T, Q, T_m) = \frac{1}{2}R + \gamma T_m$  which is a linear form of  $f(R, T_m)$  theory and it is widely investigated in past literature.

In this study, we consider the solution (35) and in this case, the function  $f(R, T, Q, T_m) = \frac{1}{2}R + \frac{\beta}{2\beta-1}T + \beta Q + \gamma T_m$ . Using this form of solution, Eqs. (29) and (30) reduce to

$$3H^2 - (\beta - 2)kH + \frac{k^2}{2}(4\beta^2 - 7\beta + 1) = (1 + \gamma)\rho - 3\gamma p \quad (36)$$

and

$$2\dot{H} + 3H^2 - \frac{3}{2}(2\beta - 3)kH - \frac{k^2}{2}(4\beta^2 - 3\beta + 2) = -(1 + 5\gamma)p - \gamma\rho, \quad (37)$$

respectively.

We choose dust fluid background source  $p = 0$ , then from Eqs. (36) and (37), we get

$$\dot{H} + k_1 H^2 - k_2 H - k_3 = 0, \quad (38)$$

with  $k_1 = \frac{3(1+2\gamma)}{2(1+\gamma)}$ ,  $k_2 = \frac{k[2(3+4\gamma)\beta - (9+13\gamma)]}{4(1+\gamma)}$  and  $k_3 = \frac{k^2[4\beta^2 - 3\beta + 2 + \gamma(8\beta^2 - 10\beta + 3)]}{2(1+\gamma)}$ .

Solving Eq. (38), we get the following Hubble function:

$$H(t) = \frac{k_2}{2k_3} + \frac{k_4}{k_3} \coth[k_4(t - c_0)], \quad (39)$$

where  $k_4 = \frac{1}{2}\sqrt{k_2^2 + 4k_1k_3}$  and  $c_0$  is an integrating constant.

Now, integrating Eq. (39), we get the scale factor  $a(t)$  as

$$a(t) = e^{k_5(t-c_1)} (\sinh[k_4(t - c_0)])^{\frac{1}{k_3}}, \quad (40)$$

where  $k_5 = \frac{k_2}{2k_3}$  and  $c_1$  is an integrating constant.

Now, for  $k_2 = 0$ , we get the hyperbolic solution

$$a(t) = \left( \sinh[\sqrt{k_1 k_3}(t - c_0)] \right)^{\frac{1}{k_3}}, \quad (41)$$

and for  $\gamma = -1$ , we get exponential solution

$$a(t) = e^{k_5(t-c_1)}. \quad (42)$$

Here, we have considered hyperbolic solution (41), and hence, we have obtained the Hubble parameter as

$$H(t) = \sqrt{\frac{k_1}{k_3}} \coth[\sqrt{k_1 k_3}(t - c_0)], \quad (43)$$

with  $\beta = \frac{9+13\gamma}{6+8\gamma}$ .

Using the relationship  $a^{-1} = 1 + z$ , we get the Hubble function in terms of  $z$  as

$$H(z) = \frac{H_0}{\sqrt{2}} \sqrt{1 + (1 + z)^{2k_3}}, \quad (44)$$

where  $H_0 = \sqrt{\frac{2k_1}{k_3}}$ .

From Eqs. (36) and (37), we obtain the energy density  $\rho$  as

$$\rho = 3H_0^2 - \frac{1}{2}k^2(4\beta + 1) + (3 - k_3)H_0^2(1 + z)^{2k_3} - \frac{1}{2\sqrt{2}}(8\beta - 13)kH_0\sqrt{1 + (1 + z)^{2k_3}}, \quad (45)$$

and total matter energy density parameter  $\Omega$  is obtained as

$$\Omega = 1 - \frac{k_3(1 + z)^{2k_3}}{3[1 + (1 + z)^{2k_3}]} - \frac{k(8\beta - 13)}{6\sqrt{2}H_0\sqrt{1 + (1 + z)^{2k_3}}} - \frac{(4\beta + 1)k^2}{6H_0^2[1 + (1 + z)^{2k_3}]}. \quad (46)$$

Now, Eqs. (36) and (37) can be rewritten as

$$3H^2 = \rho_m + \rho_{de}, \quad (47)$$

and

$$2\dot{H} + 3H^2 = -p_m - p_{de}, \quad (48)$$

where  $\rho_m = \rho$ ,  $p_m = p$ , and dark energy density  $\rho_{de}$  and pressure  $p_{de}$  is defined as

$$\rho_{de} = \gamma\rho - (\beta - 2)kH - \frac{k^2}{2}(4\beta^2 - 7\beta + 1), \quad (49)$$

and

$$p_{de} = \gamma\rho - \frac{3}{2}(2\beta - 3)kH - \frac{k^2}{2}(4\beta^2 - 3\beta + 2). \quad (50)$$

We have derived the dark energy density  $\rho_{de}$  and pressure  $p_{de}$  as

$$\rho_{de} = k_3H_0^2(1 + z)^{2k_3} + \frac{1}{2\sqrt{2}}kH_0(8\beta - 13)\sqrt{1 + (1 + z)^{2k_3}} + \frac{1}{2}(4\beta + 1), \quad (51)$$

and

$$p_{de} = -3H_0^2 - (3 - k_3)H_0^2(1 + z)^{2k_3}. \quad (52)$$

Now, the dark energy EoS parameter  $\omega_{de}$  is obtained as

$$\omega_{de} = \frac{-3H_0^2 - (3 - k_3)H_0^2(1 + z)^{2k_3}}{k_3H_0^2(1 + z)^{2k_3} + \frac{1}{2\sqrt{2}}kH_0(8\beta - 13)\sqrt{1 + (1 + z)^{2k_3}} + \frac{1}{2}(4\beta + 1)}. \quad (53)$$

## 4.1 Observational constraints

In order to determine the optimal values for the model parameters  $H_0$  and  $\gamma$  using observational datasets, we conduct a Monte Carlo Markov Chain (MCMC) analysis on a dataset comprising 31 cosmic chronometers (CC) and 1048 from the Pantheon sample of SNe Ia. This analysis is facilitated by the emcee software, which is freely accessible at [71].

### Hubble data

In the exploration of the cosmic expansion history of the universe, the Hubble data points play a vital role. We utilize 31 data points of  $H(z)$  from the CC sample [72, 73] within the range of  $0.07 \leq z \leq 1.965$ . The data points exhibit no correlation and can be analyzed using the following  $\chi^2$  formula:

$$\chi_{CC}^2 = \sum_{i=1}^{i=31} \frac{[H_{ob}(z_i) - H_{th}(H_0, \gamma, z_i)]^2}{\sigma_{H(z_i)}^2}. \quad (54)$$

where  $H_0, \gamma$  are the cosmological parameters which we have to estimate, and  $H_{ob}, H_{th}$  are the observational and theoretical values of  $H(z)$  at  $z = z_i$ , respectively. The  $\sigma_{H(z_i)}$  denotes the standard deviations associated with observed values  $H_{ob}$ .

Figure 1 illustrates the 2D contour plots of model parameters  $H_0$  and  $\gamma$  at the  $\sigma_1$  and  $\sigma_2$  levels of confidence. The estimated constrained values of  $H_0$  and  $\gamma$ , along with the minimum  $\chi$  square value, are presented in Table 1. The value of the Hubble constant has been measured as  $H_0 = 65.3_{-2.5}^{+2.1}$  km/s/Mpc for the CC dataset, aligning with recent observations.

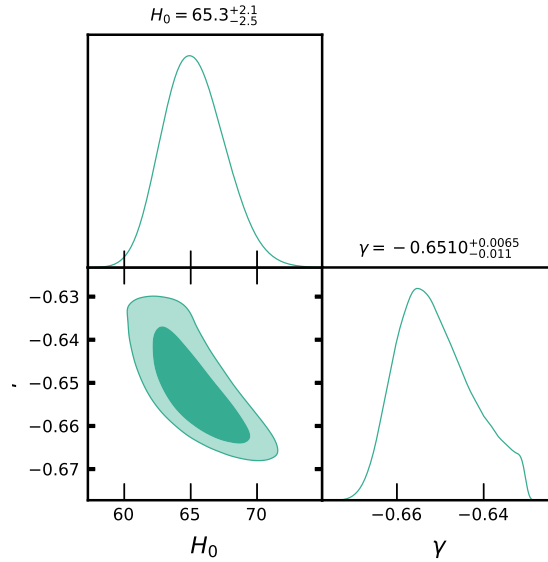


Figure 1: 2D contour plots of  $H_0, \gamma$  using MCMC analysis of 31 CC dataset.

### Pantheon data

Type Ia supernova data is employed to quantify the expansion rate of the universe's cosmic evolution, expressed as apparent magnitude  $m(z)$ . We examined the theoretical concept of apparent magnitude, as detailed in [74–77].

$$m(z) = M + 5 \log_{10} \left( \frac{D_L}{\text{Mpc}} \right) + 25. \quad (55)$$



where  $M$  denotes the absolute magnitude, and the luminosity distance  $D_L$  is measured in units of length and is defined as

$$D_L = c(1+z) \int_0^z \frac{dz'}{H(z')}. \quad (56)$$

The Hubble-free luminosity distance  $d_L$  is defined as  $d_L \equiv \frac{H_0}{c} D_L$ , representing a dimensionless quantity. Thus, the apparent magnitude  $m(z)$  is defined as

$$m(z) = M + 5 \log_{10} \left( \frac{c/H_0}{\text{Mpc}} \right) + 25 + 5 \log_{10} d_L, \quad (57)$$

$$m(z) = \mathcal{M} + 5 \log_{10} d_L. \quad (58)$$

Our analysis revealed a degeneracy between  $H_0$  and  $M$  in the previously reported equation, which maintains its invariance within the  $\Lambda$ CDM framework [74, 77]. We will integrate these degenerate parameters through a redefinition as outlined below:

$$\mathcal{M} \equiv M + 5 \log_{10} \left( \frac{c/H_0}{\text{Mpc}} \right) + 25. \quad (59)$$

In this context,  $\mathcal{M}$  represents a dimensionless parameter, defined by the equation  $\mathcal{M} = M - 5 \log_{10}(h) + 42.39$ , where  $H_0 = h \times 100$  km/s/Mpc. Within the framework of the  $\Lambda$ CDM model, the parameter  $\mathcal{M} = 23.809 \pm 0.011$  has been calibrated as outlined in reference [74]. The parameter  $\mathcal{M}$  shows differences among different cosmological theories (see [74, 80–90]). The examination of the Pantheon data is carried out utilizing the subsequent  $\chi^2$  formula, as cited in [74]:

$$\chi_P^2 = V_P^i C_{ij}^{-1} V_P^j \quad (60)$$

The formula  $V_P^i$  demonstrates the difference between the observed value  $m_{ob}(z_i)$  and the expected value  $m(\gamma, \mathcal{M}, z_i)$  as outlined in equation (58). The notation  $C_{ij}^{-1}$  represents the inverse of the covariance matrix derived from the Pantheon sample.

For the joint analysis of CC+Pantheon 1079 datasets, we use the following  $\chi$  square formula:

$$\chi_{CC+P}^2 = \chi_{CC}^2 + \chi_P^2 \quad (61)$$

Parameter	Prior	CC	CC+Pantheon
$H_0$	(50, 100)	$65.3^{+2.1}_{-2.5}$	$69.0 \pm 1.8$
$\gamma$	(−0.99, −0.63)	$-0.6510^{+0.0065}_{-0.011}$	$-0.6648^{+0.0022}_{-0.0027}$
$\mathcal{M}$	(23, 24)	-	$23.8310 \pm 0.0090$
$\chi^2$	-	14.9005	1047.7762

Table 1: The MCMC estimates.

Figure 2 presents the 2D contour plots illustrating the model parameters  $H_0$ ,  $\gamma$ , and  $\mathcal{M}$  at the confidence levels of  $\sigma_1$  and  $\sigma_2$ . The constrained estimates for  $H_0$ ,  $\gamma$ , and  $\mathcal{M}$ , along with the corresponding minimum  $\chi$  square value, are presented in Table 1. The value of the Hubble constant has been measured as  $H_0 = 69.0 \pm 1.8$  km/s/Mpc for the CC+Pantheon dataset, aligning with recent observations. Recently, in several investigations, cosmologists reported the value of the Hubble constant as  $H_0 = 68.326^{+1.005}_{-1.045}$  km/s/Mpc in [91],  $H_0 = 68.95^{+2.17}_{-0.95}$  km/s/Mpc in [92],  $H_0 = 64.75$  km/s/Mpc in [93],  $H_0 = 67.71 \pm 0.86$  km/s/Mpc in [94],  $H_0 = 68^{+2.3}_{-2.0}$  km/s/Mpc in [95]. Additional measurements of the Hubble constant yield a value of  $H_0 = 69.8 \pm 1.3$  km/s/Mpc in [96],  $H_0 = 69.7 \pm 1.2$  km/s/Mpc in [97],  $H_0 = 68.3721 \pm 1.7205$  km/s/Mpc in [98],  $H_0 = 68.3721 \pm 1.65678$  km/s/Mpc in [99], and  $H_0 = 71.66123 \pm 0.33061$  in [100]. Consequently, our estimated values for the Hubble constant fall within the range of  $64 < H_0 < 73$  based on the analysis of both datasets.

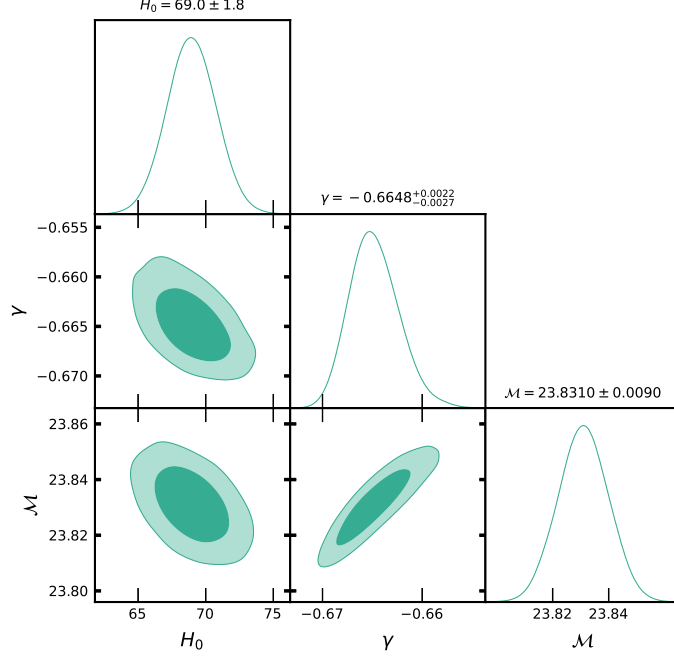


Figure 2: 2D contours of  $H_0$ ,  $\gamma$  and  $\mathcal{M}$  at  $\sigma 1$  and  $\sigma 2$  confidence level for CC+Pantheon datasets.

## 5 Result discussions

In this section, we will discuss the physical behavior of cosmological parameters and their implications in evolution of universe. The effective equation of state (EoS) is defined as  $\omega_{eff} = -1 + \frac{2}{3}(1+z)\frac{H'}{H}$  and is derived for the model as

$$\omega_{eff} = -1 + \frac{2}{3} \frac{k_3(1+z)^{2k_3}}{1 + (1+z)^{2k_3}} \quad (62)$$

where  $k_3 = \frac{k^2[4\beta^2 - 3\beta + 2 + \gamma(8\beta^2 - 10\beta + 3)]}{2(1+\gamma)}$  and  $\beta = \frac{9+13\gamma}{6+8\gamma}$ .

We have measured the value of the Hubble constant  $H_0 = 65.3_{-2.5}^{+2.1}$  km/s/Mpc and the model parameter  $\gamma = -0.6510_{-0.011}^{+0.0065}$  for the CC dataset, while for the CC+Pantheon dataset, we measured  $H_0 = 69.0 \pm 1.8$  km/s/Mpc and  $\gamma = -0.6648_{-0.0027}^{+0.0022}$ . We have used the value of the arbitrary constant  $k = 1$  in our analysis and discussion of the results. We have obtained the relationships between  $\alpha$ ,  $\beta$ , and  $\gamma$  as  $\alpha = \frac{9+13\gamma}{12+18\gamma}$  and  $\beta = \frac{9+13\gamma}{6+8\gamma}$ . So, by using the value of  $\gamma$ , we can calculate the constrained values of the other model parameters  $\alpha$  and  $\beta$  as  $\alpha = 0.6780_{-0.1184}^{+0.0583}$ ,  $0.5246_{-0.0637}^{+0.0277}$  and  $\beta = 1.9042_{-0.3466}^{+2.7862}$ ,  $10.6428_{-2.1803}^{+0.3056}$ , based on two sets of observational data, CC and CC+Pantheon.

Figure 3 illustrates the plot of the effective EoS parameter  $\omega_{eff}$  using the above estimated values of model parameters. From Figure 3, we can see that the effective EoS parameter varies as  $-1 \leq \omega_{eff} < 0$  over the redshift  $z \in [-1, \infty)$ . Also, one can see that as  $z \rightarrow \infty$ , then  $\omega_{eff} \rightarrow -1 + \frac{2}{3}k_3$ , which shows that early scenarios of the model depend upon the value of model parameters  $\alpha$ ,  $\beta$ , and  $\gamma$ . We found that the current value of the effective EoS parameter is  $\omega_{eff} = -0.55 \pm 0.16$  using CC data, and when combining CC with Pantheon data, it is estimated to be  $\omega_{eff} = -0.62 \pm 0.11$ , which is similar to the  $\Lambda$ CDM value of about  $\omega_{eff} \approx -0.70$  [2, 3].

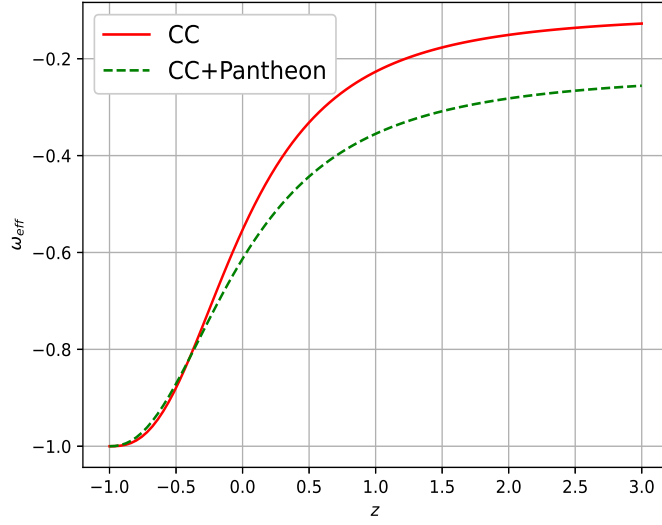


Figure 3: The variation of effective EoS parameter  $\omega_{eff}$  versus  $z$ .

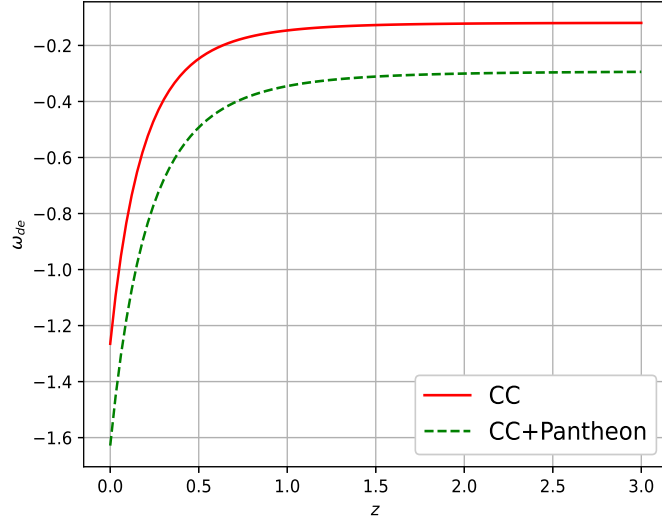


Figure 4: The variation of dark energy EoS parameter  $\omega_{de}$  versus  $z$ .

Equation (53) represents the expression for the dark energy EoS parameter, and its variation over redshift  $z$  is shown in Figure 4. From Figure 4, one can observe that the evolution of  $\omega_{de}$  over  $z$  illustrates the quintom-type scenarios of the universe's evolution. Recently, the quintom-type scenarios are extensively discussed and categorized in [101–104]. In [101], it was shown that there are two main types of quintom models: quintom-A, where a normal field is more important in the early universe and a phantom field takes over in the late universe, leading to a change from above to below the phantom divide; and quintom-B, where the equation of state moves from below  $\omega = -1$  to above  $\omega = -1$ . Thus, one can see that Figure 4 shows quintom-A-like scenarios of the model. The dark energy equation of state  $\omega_{de}$  is reported as  $\omega_{de} = -0.98 \pm 0.12$  in [105], while it is measured as  $\omega_{de} = -1.0 \pm 0.19$  and  $\omega_{de} = -1.10 \pm 0.14$  in [106]. We have measured the present value of this dark energy EoS parameter as  $\omega_{de} = -1.2648$  along CC data, while for CC+Pantheon datasets  $\omega_{de} = -1.6285$ .

The deceleration parameter is defined as  $q(z) = -1 + (1+z)\frac{H'}{H}$  and is derived for the model as

$$q(z) = -1 + \frac{k_3(1+z)^{2k_3}}{1 + (1+z)^{2k_3}} \quad (63)$$

where  $k_3 = \frac{k^2[4\beta^2 - 3\beta + 2 + \gamma(8\beta^2 - 10\beta + 3)]}{2(1+\gamma)}$  and  $\beta = \frac{9+13\gamma}{6+8\gamma}$ . Figure 5 depicts the variation of  $q(z)$  versus  $z$ . From Figure 5, we see that as  $z \rightarrow -1$ ,  $q \rightarrow -1$ , while for  $z \rightarrow \infty$ ,  $q \rightarrow (k_3 - 1)$ , which may be a positive or negative value according to the value of  $k_3$ . Thus, the derived model can explain both scenarios of the expanding universe, like the early decelerating and late-time accelerating phases. We have estimated the present value of  $q(z)$  as  $q_0 = -0.3296$  along CC data and  $q_0 = -0.4195$  for CC+Pantheon data, which reveals the current accelerating phase of the universe. Figure 5 illustrates a phenomenon known as signature-flipping in the evolution of  $q(z)$ , which is referred to as the transition point  $z_t$ . This transition redshift  $z_t$  is derived from  $q(z_t) = 0$ , as

$$z_t = \left[ \frac{1}{k_3 - 1} \right]^{\frac{1}{2k_3}} - 1 \quad (64)$$

Recently, several cosmologists have reported the value of this transition redshift  $z_t$  as  $z_t = 0.8596^{+0.2886}_{-0.2722}$  along the SNe Ia dataset and  $z_t = 0.6320^{+0.1605}_{-0.1403}$  along the Hubble data in [107]. One is reported as  $z_t = 0.643^{+0.034}_{-0.030}$  in [108], while [109] is obtained as  $z_t = 0.646^{+0.020}_{-0.158}$  and  $z_t = 0.702^{+0.094}_{-0.044}$  in [110]. In another work, it is reported as  $z_t = 0.684^{+0.136}_{-0.092}$  [111, 112]. We have measured the transition redshift  $z_t = 0.4944$  for CC data, while along CC+Pantheon data, it is estimated as  $z_t = 1.196$ . Thus, in comparison to the above results, our measured value of transition redshift  $z_t$  is consistent with observational datasets.

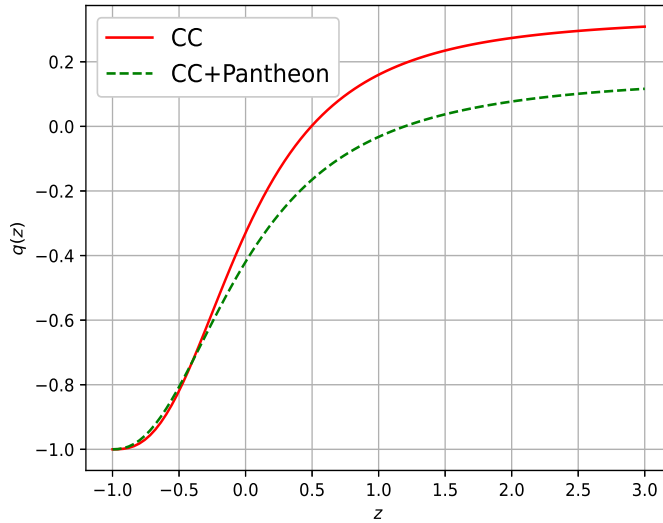


Figure 5: The variation of deceleration parameter  $q(z)$  versus  $z$ .

## 5.1 Om diagnostic

The Om diagnostic function classifies cosmic dark energy ideas by behavior. The Om diagnostic function is defined for a spatially homogeneous universe [113].

$$Om(z) = \frac{\left( \frac{H(z)}{H_0} \right)^2 - 1}{(1+z)^3 - 1}, \quad (65)$$

where  $H_0$  represents the present value of the Hubble parameter, and  $H(z)$  denotes the Hubble parameter as outlined in Eq.(44). A positive slope of  $Om(z)$  indicates phantom motion, whereas a negative slope signifies quintessence motion. The LambdaCDM model is characterized by the constant  $Om(z)$ .

Equation (65) delineates the  $Om(z)$  function for the model we formulated, while Figure 6 depicts its geometric interpretation. Figure 6 illustrates that  $Om(z)$  ascends with an increase in  $z$ , signifying a positive gradient. This indicates that our universe model has characteristics akin to a phantom dark energy hypothesis. Furthermore, it is evident that when  $z \rightarrow -1$  in the distant future, the value of  $Om(z)$  remains constant, indicating the convergence of our derived model towards the  $\Lambda$ CDM model in the far future.

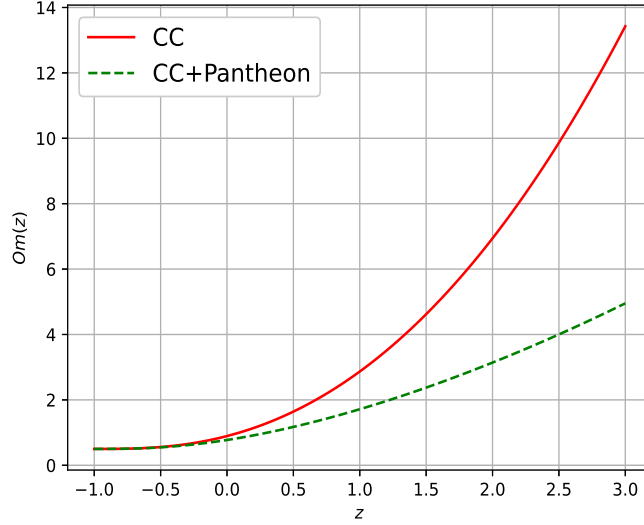


Figure 6: The variation of  $Om(z)$  function versus  $z$ .

## 5.2 Age of the Universe

To calculate the age of the universe, we apply the formula below:

$$t_0 - t = \int_0^z \frac{dz'}{(1+z')H(z')} \quad (66)$$

By employing the Hubble function expression (44) in (66), we derive the age of the universe as

$$t_0 = \lim_{z \rightarrow \infty} (t_0 - t) = \lim_{z \rightarrow \infty} \left[ \frac{\sqrt{2}}{H_0} \int_0^z \frac{dz'}{(1+z')\sqrt{1+(1+z')^{2k_3}}} \right] \quad (67)$$

As  $z \rightarrow \infty$ ,  $t \rightarrow 0$ , and  $(t_0 - t) \rightarrow t_0$ , this represents the current age of the universe. The current estimation of the universe's age is  $t_0 = 13.92 \pm 1.3$  Gyrs based on CC data, whereas for CC+Pantheon data, it is  $t_0 = 13.87 \pm 1.02$  Gyrs. Recent observations indicate that the current age of the universe is reported as  $t_0 = 13.7 \pm 0.02$  Gyr in [105], while another source provides an age of  $t_0 = 13.772 \pm 0.059$  Gyr in [114]. Consequently, our calculated value for the current age aligns closely with observational findings.

## 6 Conclusions

The current transit universe model constitutes an exact solution to the field equations of a recently introduced Metric-affine Myrzakulov  $f(R, T, Q, T_m)$  gravity theory [Herko et al. *Phys. Dark Univ.* **34** (2021) 100886]. We

formulate a hyperbolic solution and derive the observational constraints on the model parameters utilizing the most recent observational datasets. We examine the evolution of cosmological parameters, including the deceleration parameter  $q(z)$ , the effective equation of state parameter  $\omega_{eff}$ , the dark energy equation of state parameter  $\omega_{de}$ , to elucidate the characteristics of the observable universe. We do the Om diagnostic test for the model, which encapsulates the quintom-A-type scenarios of the model.

We have measured the value of the Hubble constant  $H_0 = 65.3^{+2.1}_{-2.5}$  km/s/Mpc and the model parameter  $\gamma = -0.6510^{+0.0065}_{-0.011}$  for the CC dataset, while for the CC+Pantheon dataset, we measured  $H_0 = 69.0 \pm 1.8$  km/s/Mpc and  $\gamma = -0.6648^{+0.0022}_{-0.0027}$ . We have used the value of the arbitrary constant  $k = 1$  in our analysis and discussion of the results. We have obtained the relationships between  $\alpha$ ,  $\beta$ , and  $\gamma$  as  $\alpha = \frac{9+13\gamma}{12+18\gamma}$  and  $\beta = \frac{9+13\gamma}{6+8\gamma}$ . So, by using the value of  $\gamma$ , we can calculate the constrained values of the other model parameters  $\alpha$  and  $\beta$  as  $\alpha = 0.6780^{+0.0583}_{-0.1184}$ ,  $0.5246^{+0.0277}_{-0.0637}$  and  $\beta = 1.9042^{+2.7862}_{-0.3466}$ ,  $10.6428^{+0.3056}_{-2.1803}$ , based on two sets of observational data, CC and CC+Pantheon. Using the above estimations, we found a transit phase quintom-A-type universe model with the current value of deceleration parameter  $q(z)$  as  $q_0 = -0.3296$  along CC data and  $q_0 = -0.4195$  for CC+Pantheon data, which reveals the current accelerating phase of the universe. We have measured the transition redshift  $z_t = 0.4944$  for CC data, while along CC+Pantheon data, it is estimated as  $z_t = 1.196$ , which is consistent with the recent estimations in [107–112].

We found that the current value of the effective EoS parameter is  $\omega_{eff} = -0.55 \pm 0.16$  using CC data, and when combining CC with Pantheon data, it is estimated to be  $\omega_{eff} = -0.62 \pm 0.11$ , which is similar to the  $\Lambda$ CDM value of about  $\omega_{eff} \approx -0.70$  [2, 3]. We have measured the present value of the dark energy EoS parameter as  $\omega_{de} = -1.2648$  along CC data, while for CC+Pantheon datasets  $\omega_{de} = -1.6285$ , and we found that the evolution of the dark energy EoS parameter  $\omega_{de}$  of the model behaves just like a quintom-A universe. The Om diagnostic test indicates that our derived model is a phantom dark energy model. The current estimation of the universe's age is  $t_0 = 13.92 \pm 1.3$  Gyrs based on CC data, whereas for CC+Pantheon data, it is  $t_0 = 13.87 \pm 1.02$  Gyrs.

Thus, the metric-affine Myrzakulov  $f(R, T, Q, T_m)$  gravity theory may be helpful in explaining quintom-like universes, which could encourage cosmologists to further investigate it.

## Acknowledgments

We express our gratitude to Inter-University Centre for Astronomy and Astrophysics (IUCAA), Pune, India for providing the resources and assistance necessary to finish this work.

## 7 Data Availability Statement

No data associated in the manuscript.

## References

- [1] C. M. Will, The confrontation between general relativity and experiment, *Living Rev. Relativ.* **17**: 4 (2014).
- [2] A. G. Riess, *et al.*, Observational evidence from supernovae for an accelerating universe and a cosmological constant, *Astron. J.*, **116**: 1009 (1998).
- [3] S. Perlmutter, *et al.*, Measurements of Omega and Lambda from 42 High-Redshift Supernovae, *Astrophys. J.*, **517**: 565 (1999).

- [4] S. Alam *et al.* (BOSS Collaboration), The clustering of galaxies in the completed SDSS-III Baryon Oscillation Spectroscopic Survey: cosmological analysis of the DR12 galaxy sample, *Mon. Not. R. Astron. Soc.*, **470**: 2617 (2017). arXiv:1607.03155.
- [5] T.M.C. Abbott *et al.* (DES Collaboration), Dark Energy Survey year 1 results: Cosmological constraints from galaxy clustering and weak lensing, *Phys. Rev. D*, **98**: 043526 (2018).
- [6] M. Tanabashi *et al.* (Particle Data Group), Review of Particle Physics: particle data groups, *Phys. Rev. D*, **98**: 030001 (2018).
- [7] N. Aghanim *et al.* (Planck Collaboration), Planck 2018 results. VI. Cosmological parameters, *Astron. Astrophys.*, **641**: A6 (2020).
- [8] E. N. Saridakis, *et al.*, Modified gravity and cosmology, arXiv:2105.12582v2 [gr-qc].
- [9] T. P. Sotiriou and V. Faraoni,  $f(R)$  theories of gravity, *Rev. Mod. Phys.*, **82**: 451-497 (2010). arXiv:0805.1726.
- [10] D. Iosifidis, A. C. Petkou, and C. G. Tsagas, Torsion/nonmetricity duality in  $f(R)$  gravity, *Gen. Relativ. Gravit.* **51**: 66 (2019).
- [11] S. Capozziello and S. Vignolo, Metric-affine  $f(R)$ -gravity with torsion: an overview, *Annalen der Physik*, **19**: 238-248 (2010).
- [12] R. Aldrovandi and J. G. Pereira, Teleparallel gravity: an introduction, (Springer Science & Business Media, 2012), volume 173, p. 214.
- [13] R. Myrzakulov, Accelerating universe from  $F(T)$  gravity, *Eur. Phys. J. C*, **71**: 1-8 (2011).
- [14] J. Beltrán Jiménez, *et al.*, Cosmology in  $f(Q)$  geometry, *Phys. Rev. D*, **2**: 103507 (2020).
- [15] J. M. Nester and H.-J. Yo, Symmetric teleparallel general relativity, arXiv:gr-qc/9809049.
- [16] J. Beltrán Jiménez, L. Heisenberg, and T. S. Koivisto, Teleparallel palatini theories, *J. Cosmo. Astropart. Phys.*, **2018**: 039 (2018).
- [17] L. Heisenberg, Review on  $f(Q)$  gravity, arXiv:2309.15958 [gr-qc].
- [18] N. Bartolo and M. Pietroni, Scalar-tensor gravity and quintessence, *Phys. Rev. D*, **61**: 023518 (1999).
- [19] C. Charmousis, *et al.*, General second-order scalar-tensor theory and self-tuning, *Phys. Rev. Lett.*, **108**: 051101 (2012).
- [20] L. P. Eisenhart, Non-Riemannian geometry, Courier Corporation, (2012).
- [21] F. W. Hehl, *et al.*, Metric-affine gauge theory of gravity: field equations, Noether identities, world spinors, and breaking of dilation invariance, *Phys. Rep.*, **258**: 1-171 (1995).
- [22] T. P. Sotiriou,  $f(R)$  gravity, torsion and non-metricity, *Class. Quant. Grav.*, **26**: 152001 (2009).
- [23] V. Vitagliano, T. P. Sotiriou and S. Liberati, Metric-affine  $f(R)$  theories of gravity, *Annals Phys.*, **326**: 1259 (2011) [Erratum-ibid. 329, 186 (2013)].
- [24] V. Vitagliano, T. P. Sotiriou and S. Liberati, Dynamics of generalized Palatini theories of gravity, *Phys. Rev. D*, **82**: 084007 (2010).
- [25] F. W. Hehl, E. A. Lord and L. L. Smalley, Metric-affine variational principles in general relativity II. Relaxation of the Riemannian constraint, *Gen. Rel. Grav.* **13**: 1037 (1981).



- [26] Vincenzo Vitagliano, The role of nonmetricity in metric-affine theories of gravity, *Class. Quantum Grav.*, **31**: 045006 (2014).
- [27] D. Iosifidis, Riemann tensor and Gauss–Bonnet density in metric-affine cosmology, *Class. Quantum Grav.*, **38**: 195028 (2021). arXiv:2104.10192.
- [28] D. Iosifidis, Cosmic acceleration with torsion and non-metricity in Friedmann-like universes, *Class. Quantum Grav.*, **38**(1): 015015 (2020).
- [29] D. Iosifidis, Cosmological hyperfluids, torsion and non-metricity, *Eur. Phys. J. C*, **80**(11): 1042 (2020).
- [30] D. Iosifidis and L. Ravera, The cosmology of quadratic torsionful gravity, *Eur. Phys. J. C*, **81**: 736 (2021).
- [31] J. Beltrán Jiménez and T. S. Koivisto, Spacetimes with vector distortion: Inflation from generalised Weyl geometry, *Phys. Lett. B*, **756**: 400–404 (2016).
- [32] J. Beltrán Jiménez and T. S. Koivisto, Modified gravity with vector distortion and cosmological applications, *Universe*, **3**(2): 47 (2017).
- [33] D. Kranas, *et al.*, Friedmann-like universes with torsion, *Eur. Phys. J. C*, **79**(4): 341 (2019).
- [34] C. Barragán, G. J. Olmo, and H. Sanchis-Alepuz, Bouncing cosmologies in Palatini  $f(R)$  gravity, *Phys. Rev. D*, **80**(2): 024016 (2009).
- [35] K. Shimada, K. Aoki, and Kei-ichi Maeda, Metric-affine gravity and inflation, *Phys. Rev. D*, **99**(10): 104020 (2019).
- [36] M. Kubota, *et al.*, Cosmological perturbations in Palatini formalism, *J. Cosmo. Astropart. Phys.*, **2021**(03): 006 (2021).
- [37] Y. Mikura, Y. Tada, and S. Yokoyama, Conformal inflation in the metric-affine geometry, *EPL*, **132**(3): 39001 (2020).
- [38] Y. Mikura, Y. Tada, and S. Yokoyama, Minimal k-inflation in light of the conformal metric-affine geometry, *Phys. Rev. D*, **103**: 101303 (2021). arXiv:2103.13045.
- [39] F. W. Hehl, G. D. Kerlick, and P. von der Heyde, On hypermomentum in general relativity I. The notion of hypermomentum, *Zeitschrift fuer Naturforschung A*, **31**(2): 111-114 (1976).
- [40] OV Babourova and BN Frolov, The variational theory of perfect fluid with intrinsic hypermomentum in space-time with nonmetricity, arXiv:gr-qc/9509013.
- [41] Y. N. Obukhov and R. Tresguerres, Hyperfluid—a model of classical matter with hypermomentum, *Phys. Lett. A*, **184**(1): 17-22 (1993).
- [42] D. Iosifidis, The perfect hyperfluid of metric-affine gravity: the foundation, *JCAP*, **04**: 072 (2021).
- [43] A. Conroy and T. Koivisto, The spectrum of symmetric teleparallel gravity, *Eur. Phys. J. C*, **78**: 923 (2018). arXiv:1710.05708.
- [44] R. Myrzakulov, FRW cosmology in  $F(R, T)$  gravity, *Eur. Phys. J. C*, **72**: 2203 (2012). arXiv:1207.1039.
- [45] E. N. Saridakis, *et al.*, Cosmological applications of gravity with dynamical curvature and torsion, *Phys. Rev. D*, **102**: 023525 (2020). arXiv:1912.03882.
- [46] M. Jamil, *et al.*, Reconstruction of some cosmological models in  $f(R, T)$  cosmology, *Eur. Phys. J. C*, **72**: 1999 (2012). arXiv:1107.5807.



- [47] M. Sharif, S. Rani and R. Myrzakulov, Analysis of  $F(R, T)$  gravity models through energy conditions, *Eur. Phys. J. Plus*, **128**: 123 (2013). arXiv:1210.2714.
- [48] S. Capozziello, M. De Laurentis and R. Myrzakulov, Noether Symmetry Approach for teleparallel-curvature cosmology, *Int. J. Geom. Meth. Mod. Phys.*, **12**: 1550095 (2015) [arXiv:1412.1471].
- [49] P. Feola, *et al.*, Mass-radius relation for neutron stars in  $f(R) = R + \alpha R^2$  gravity: A comparison between purely metric and torsion formulations, arXiv:1909.08847.
- [50] F.K. Anagnostopoulos, S. Basilakos, and E.N. Saridakis, Observational constraints on Myrzakulov gravity, *Phys. Rev. D*, **103**: 104013 (2021). arXiv:2012.06524[gr-qc].
- [51] N. Myrzakulov, R. Myrzakulov, L. Ravera, Metric-affine Myrzakulov gravity theories, arXiv:2108.00957.
- [52] D. Iosifidis, N. Myrzakulov, R. Myrzakulov, Metric-Affine Version of Myrzakulov  $F(R, T, Q, \mathcal{T})$  Gravity and Cosmological Applications, *Universe*, **7**: 262 (2021). arXiv:2106.05083.
- [53] T. Harko, *et al.*, Non-minimal geometry–matter couplings in Weyl–Cartan space–times:  $f(R, T, Q, T_m)$  gravity, arxiv:2110.00358v1.
- [54] R. Saleem, Aqsa Saleem, Viable constraints on some Myrzakulov  $f(R, T, Q, T_m)$  models to study Baryon asymmetry, *Chin. J. Phys.*, **84**: 471-485 (2023).
- [55] D. Iosifidis, *et al.*, Metric-affine vector–tensor correspondence and implications in  $F(R, T, Q, T, D)$  gravity, arXiv:2111.14214.
- [56] G. Papagiannopoulos, S. Basilakos, E.N. Saridakis, Dynamical system analysis of Myrzakulov gravity, arXiv:2202.10871.
- [57] S. Kazempour, A. R. Akbarieh, Cosmological study in Myrzakulov  $F(R, T)$  quasi-dilaton massive gravity, arXiv:2309.09230.
- [58] T. Harko, N. Myrzakulov, R. Myrzakulov, S. Shahidi, Non-minimal geometry-matter couplings in Weyl–Cartan space-times:  $f(R, T, Q, T_m)$  gravity, *Phys. Dark Univ.* **34** (2021) 100886,
- [59] D. C. Maurya, R. Myrzakulov, Transit cosmological models in  $F(R, \bar{T})$  gravity theory, *Eur. Phys. J. C*, **84**: 534 (2024). arXiv:2401.00686.
- [60] D. C. Maurya, R. Myrzakulov, Exact cosmological models in metric-affine  $F(R, T)$  gravity, *Eur. Phys. J. C*, **84**: 625 (2024). arXiv:2402.02123.
- [61] D. C. Maurya, *et al.*, Metric-Affine  $F(T, Q)$  gravity: cosmological implications and constraints, arXiv:2404.09698[gr-qc].
- [62] D. C. Maurya, K. Yesmakhanova, R. Myrzakulov, G. Nugmanova, FLRW Cosmology in Metric-Affine  $F(R, Q)$  Gravity, *Chinese Physics C*, **48**(12) (2024) 125101.
- [63] H. A. Buchdahl, Non-linear Lagrangians and cosmological theory, *Mon. Not. Roy. Astron. Soc.*, **150**, 1 (1970).
- [64] R. Aldrovandi and J. G. Pereira, Teleparallel Gravity, Fundamental Theories of Physics 173, Springer, Heidelberg, 2013.
- [65] J. Beltrán Jiménez, L. Heisenberg, and T. Koivisto, Coincident general relativity, *Phys. Rev. D*, **98**, 044048 (2018).
- [66] T. Harko, F. S. N. Lobo, S. Nojiri and S. D. Odintsov,  $f(R, T)$ -gravity, *Phys. Rev. D* **84**, 024020 (2011).

- [67] T. Harko, F. S. N. Lobo, G. Otalora, and E. N. Saridakis,  $f(T, \mathcal{T})$  gravity and cosmology, *JCAP* **12**, 021 (2014).
- [68] Y. Xu, G. Li, T. Harko, and S.-D. Liang, Regular article-theoretical physics, *Eur. Phys. J. C* **79**, 708 (2019).
- [69] Y. Xu, T. Harko, S. Shahidi, and S.-D. Liang, Weyl type  $f(Q, T)$  gravity, and its cosmological implications, *Eur. Phys. J. C* **80**, 449 (2020).
- [70] D. Iosifidis, N. Myrzakulov, and R. Myrzakulov, Metric-Affine Version of Myrzakulov  $F(R, T, Q, \mathcal{T})$  Gravity and Cosmological Applications, *Universe* **7**, 262 (2021).
- [71] D. Foreman-Mackey, D.W. Hogg, D. Lang, *et al.*, emcee: the MCMC hammer, *Publ. Astron. Soc. Pac.*, **125**: 306 (2013). <https://doi.org/10.1086/670067>
- [72] J. Simon, L. Verde, R. Jimenez, Constraints on the redshift dependence of the dark energy potential, *Phys. Rev. D* **71** 123001 (2005).
- [73] G. S. Sharov, V. O. Vasiliev, How predictions of cosmological models depend on Hubble parameter data sets, *Math. Model. Geom.* **6**, 1-20 (2018).
- [74] K. Asvesta, L. Kazantzidis, L. Perivolaropoulos, C.G. Tsagas, Observational constraints on the deceleration parameter in a tilted universe, *Mon. Not. R. Astron. Soc.* **513**, 2394-2406 (2022).
- [75] D.W. Hogg and D.F. Mackey, Data analysis recipes: Using Markov Chain Monte Carlo, *The Astrophysical Journal Supplement Series* **236** (2018) 18. [arXiv:1710.06068 [astro-ph.IM]].
- [76] R. Jimenez and A. Loeb, Constraining Cosmological Parameters Based on Relative Galaxy Ages, *ApJ* **573** (2002) 37.
- [77] G. Ellis, R. Maartens, M. MacCallum, Relativistic Cosmology (Cambridge University Press, Cambridge, 2012). <https://doi.org/10.1017/CBO9781139014403>.
- [78] A. Conley et al., Supernova constraints and systematic uncertainties from the first three years of the supernova legacy survey\*, *ApJ* **192** (2011) 1.
- [79] D. M. Scolnic et al., The Complete Light-curve Sample of Spectroscopically Confirmed SNe Ia from Pan-STARRS1 and Cosmological Constraints from the Combined Pantheon Sample, *ApJ* **859** (2018) 101.
- [80] Dong Zhao, Yong Zhou, Zhe Chang, Anisotropy of the Universe via the Pantheon supernovae sample revisited, *MNRAS* **486** (2019) 5679-5689, <https://doi.org/10.1093/mnras/stz1259>.
- [81] L. Kazantzidis, L. Perivolaropoulos, Hints of a local matter underdensity or modified gravity in the low  $z$  Pantheon data, *Phys. Rev. D* **102** (2020) 023520, <https://link.aps.org/doi/10.1103/PhysRevD.102.023520>.
- [82] D. Sapone, et al., Is there any measurable redshift dependence on the SN Ia absolute magnitude?, *Phys. Dark Univ.* **32** (2021) 100814.
- [83] L. Kazantzidis, H. Koo, S. Nesseris, L. Perivolaropoulos, A. Shafieloo, Hints for possible low redshift oscillation around the best-fitting  $\Lambda$ CDM model in the expansion history of the Universe, *MNRAS* **501** (2021) 3421-3426, <https://doi.org/10.1093/mnras/staa3866>.
- [84] M. G. Dainotti et al., On the Hubble Constant Tension in the SNe Ia Pantheon Sample, *ApJ* **912** (2021) 150.
- [85] M. G. Dainotti et al., On the Evolution of the Hubble Constant with the SNe Ia Pantheon Sample and Baryon Acoustic Oscillations: A Feasibility Study for GRB-Cosmology in 2030, *Galaxies* **10** (2022) 24; <https://doi.org/10.3390/galaxies10010024>.

- [86] G. Alestas, L. Kazantzidis, L. Perivolaropoulos,  $w - M$  phantom transition at  $z_t \simeq 0.1$  as a resolution of the Hubble tension, *Phys. Rev. D* **103** (2021) 083517.
- [87] D. Camarena, V. Marra, On the use of the local prior on the absolute magnitude of Type Ia supernovae in cosmological inference, *MNRAS* **504** (2021) 5164-5171, <https://doi.org/10.1093/mnras/stab1200>.
- [88] V. Marra, L. Perivolaropoulos, Rapid transition of  $G_{\text{eff}}$  at  $z_t \simeq 0.01$  as a possible solution of the Hubble and growth tensions, *Phys. Rev. D* **104** (2021) L021303.
- [89] G. Alestas, I. Antoniou L. Perivolaropoulos, Hints for a Gravitational Transition in Tully-Fisher Data, *Universe* **7** (2021) 366; <https://doi.org/10.3390/universe7100366>.
- [90] L. Perivolaropoulos, Is the Hubble crisis connected with the extinction of dinosaurs?, arXiv:2201.08997 [astro-ph.EP].
- [91] G. P. Singh, R. Garg, A. Singh, A generalized  $\Lambda$ CDM model with parameterized Hubble parameter in particle creation, viscous and  $f(R)$  model framework, [arXiv:2405.15626 [gr-qc]].
- [92] A. Pradhan, D. C. Maurya, G. K. Goswami, A. Beesham, Modeling Transit Dark Energy in  $F(R, L_m)$ -gravity, *Int. J. Geom. Meth. Mod. Phys.*, **20**(06) 2350105 (2023), [arXiv:2209.14269 [gr-qc]]
- [93] D. C. Maurya, Accelerating scenarios of massive universe in  $f(R, L_m)$ -gravity, *New Astronomy* **100**, 101974 (2023)
- [94] D. C. Maurya, Bianchi-I dark energy cosmological model in  $f(R, L_m)$ -Gravity, *Int. J. Geom. Meth. Mod. Phys.* **21**(04) 2450072-194 (2024)
- [95] D. C. Maurya, Constrained  $\Lambda$ CDM Dark Energy Models in Higher Derivative  $F(R, L_m)$ -Gravity Theory, *Phys. Dark Universe* **42** (2023) 101373
- [96] S. Cao and B. Ratra,  $H_0 = 69.8 \pm 1.3 \text{ km s}^{-1} \text{ Mpc}^{-1}$ ,  $\Omega_{m0} = 0.288 \pm 0.017$ , and other constraints from lower-redshift, non-CMB, expansion-rate data, *Phys. Rev. D* **107**, 103521 (2023). [arXiv:2302.14203 [astro-ph.CO]].
- [97] S. Cao and B. Ratra, Using lower-redshift, non-CMB, data to constrain the Hubble constant and other cosmological parameters, *MNRAS* **513**, 5686-5700 (2022). [arXiv:2203.10825 [astro-ph.CO]].
- [98] D.C. Maurya and J. Singh, Modified  $f(Q)$ -Gravity String Cosmological Models With Observational Constraints, *Astronomy and Computing* **46** 100789 (2024).
- [99] D.C. Maurya, A. Dixit, and A Pradhan, Transit string dark energy models in  $f(Q)$  gravity, *Inter. J. Geom. Meth. Mod. Phys.* **20** 2350134 (2023).
- [100] D.C. Maurya, Phantom Dark Energy Nature of String-Fluid Cosmological Models in  $f(Q)$ -Gravity, *Gravitation and Cosmology* **29** (4), 345-361 (2023).
- [101] Z.K. Guo, et al., Two-field quintom models in the  $w - w'$  plane, *Phys. Rev. D* **74** (2006) 127304.
- [102] Cai Yi-Fu, et al., Quintom cosmology: Theoretical implications and observations, *Physics Reports*, **493**(1) 1-60 (2010).
- [103] Yang Yuhang, Quintom cosmology and modified gravity after DESI 2024, *Science Bulletin*, **69**(17) 2698-2704 (2024).
- [104] Cai Yi-Fu, et al., The Quintom theory of dark energy after DESI DR2, arXiv:2505.24732 [astro-ph.CO].

- [105] D.N. Spergel, *et al.*, First-year Wilkinson Microwave Anisotropy Probe (WMAP)\* observations: determination of cosmological parameters, *Astrophys. J. Suppl.*, **148**, 175 (2003).
- [106] E. Komatsu, *et al.*, Seven-Year Wilkinson Microwave Anisotropy Probe (WMAP) Observations: Cosmological Interpretation, *Astrophys. J. Suppl.*, **192**(2), 18 (2011).
- [107] S. Capozziello, O. Farooq, O. Luongo, *et al.*, Cosmographic bounds on the cosmological deceleration-acceleration transition redshift in  $f(R)$  gravity, *Phys. Rev. D* **90**, 044016 (2014), [arXiv:1403.1421v1 [gr-qc]].
- [108] S. Capozziello, O. Luongo, E. N. Saridakis, Transition redshift in  $f(T)$  cosmology and observational constraints, *Phys. Rev. D* **91** 124037 (2015), [arXiv:1503.02832v2 [gr-qc]].
- [109] S. Capozziello, P. K. S. Dunsby, O. Luongo, Model independent reconstruction of cosmological accelerated-decelerated phase, *MNRAS* **509** (2022) 5399-5415, [arXiv:2106.15579v2 [astro-ph.CO]].
- [110] M. Muccino, O. Luongo, D. Jain, Constraints on the transition redshift from the calibrated Gamma-ray Burst Ep-Eiso correlation, *MNRAS* **523** (2023) 4938-4948, [arXiv:2208.13700v3 [astro-ph.CO]].
- [111] A. C. Alfano, S. Capozziello, O. Luongo, *et al.*, Cosmological transition epoch from gamma-ray burst correlations, (2024) [arXiv:2402.18967v1 [astro-ph.CO]].
- [112] A. C. Alfano, C. Cafaro, S. Capozziello, *et al.*, Dark energy-matter equivalence by the evolution of cosmic equation of state, *Phys. Dark Univ.* **42** 101298 (2023), [arXiv:2306.08396v2 [astro-ph.CO]].
- [113] V. Sahni, A. Shafieloo, A. A. Starobinsky, Two new diagnostics of dark energy, *Phys. Rev. D* **78** (2008) 103502.
- [114] C. L. Bennett *et al.*, NINE-YEAR WILKINSON MICROWAVE ANISOTROPY PROBE(WMAP) OBSERVATIONS: FINAL MAPS AND RESULTS, *ApJS* **208** 20 (2013).